Computation of the Strain Induced Critical Current Reduction in the 16 T Nb_3Sn Test Facility Dipole

G. Vallone, E. Anderssen, D. Arbelaez, N. Cheggour, P. Ferracin, GL. Sabbi, D. Turrioni

***Abstract*—A test facility dipole is being developed at LBNL, targeting a 16 T field in a 144 mm wide aperture. The magnet uses a block design, with two double-pancake coils. In order to minimize motion under the large Lorentz forces, the coils are preloaded against a thick aluminum shell and iron yoke using bladder and key technology. It is then crucial to verify that the performance of the magnet is not degraded due to strain induced on the Nb_3Sn conductor during assembly, cool-down and powering. The critical current of extracted strands was measured in a varying background magnetic field and as a function of the applied longitudinal strain. Finite element analysis was used to extract the strain state inside the superconducting strands during magnet assembly and operation. This strain was then compared to the measurements to evaluate potential reversible and irreversible effects on the magnet performances. The results suggest that the magnet can reach 16 T with sufficient margin, with no irreversible degradation in the high field region.**

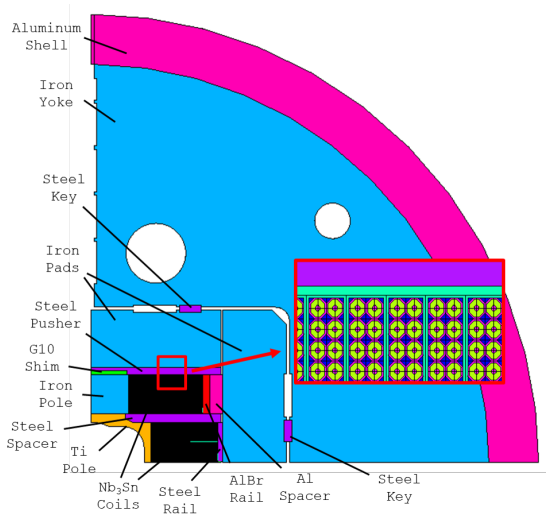

Fig. 1. TFD cross-section, along with the FE modeling strategy used to represent separately the superconducting regions in each strand.

TABLE I
STRAND AND CABLE PARAMETERS

Parameter	Value
Wire Diameter [mm]	1.1
Cu to non-Cu ratio	0.9
Wire Architecture	RRP 162/169
Cabling Degradation [%]	5
Number of Strands	44
Cable Width †	26.2 mm
Cable Thickness †	1.95 mm
Insulation Thickness	0.15 mm

† After heat treatment.

I. INTRODUCTION

STRAIN induced effects on the critical surface of Nb_3Sn conductors can be predicted, within the reversible region, using to the scaling laws developed on longitudinally loaded strands. Among these, the exponential scaling law, proposed in [1], introduces the dependence of the critical surface not only on the longitudinal strain but on the full strain tensor. The law was initially developed on uni-axial longitudinal loads on single strands. More recently, it was shown that this law can be used to also match the reversible critical current reduction of strand and cables under transversal loads [2], [3]. In [4], a methodology was introduced to compute the actual limits of superconducting magnets under applied strains.

Until now, this methodology was applied only once on a Nb_3Sn quadrupole with a $\cos\theta$ design. Here, we use it on a Test Facility Dipole (TFD) that is being developed at the Lawrence Berkeley National Laboratory. The dipole aims at an ambitious 16 T field in a 144 mm wide aperture. Because of the very large field and aperture, large stresses/strains will be applied to the coils, making an accurate verification of their effects on the critical surface of foremost importance. In the past, test facility magnets were designed applying empirical limits on the horizontal [5] or Von Mises equivalent stress [6]. These limits were established comparing FE models, where the coils were represented as blocks of an homogeneous material, with magnet test results [7]. In this paper, we parametrize the critical surface using measurements on uniaxially loaded strands; then, we evaluate the magnet current limit including the impact of mechanical strains on the critical surface. For the first time, we also define an irreversible limit for non-uniaxial mechanical strains, using the exponential strain function.

II. THE TEST FACILITY DIPOLE

The Test Facility Dipole (TFD), is designed for the test of fusion and accelerator cables [8]. The magnet, shown in Fig.

This work was supported by the High Luminosity LHC Project at CERN and by the DOE through the U.S. LHC Accelerator Research Program.

G. Vallone, E. Anderssen, D. Arbelaez, P. Ferracin and GL. Sabbi are with Lawrence Berkeley National Laboratory, Berkeley, CA 94720 USA (e-mail: gvallone@lbl.gov).

N. Cheggour is with National High Magnetic Field Laboratory, Tallahassee, Fl, USA.

D. Turrioni is with Fermi National Accelerator Laboratory, Batavia, IL, USA.

1, targets a 16 T field in a 144 wide mm aperture. The nominal current is equal to 16.03 kA. Four superconducting coils in a double-pancake configuration are wound using a wide cable (26.2 mm) in order to maximize the field and minimize the stress. The main strand and cable parameters are presented in Table I. The coils are separated by a thick steel shim to reduce the titanium pole bending, the stress in the coils, and to minimize the tension between the coil and poles. The magnet uses the bladder and key technology to provide the horizontal prestress [9]. Horizontal and vertical keys are inserted between the iron yoke and iron pads. Detailed magnetic, mechanical and protection analysis can be found in [8], [10], [11].

III. Methodology Overview

To compute the effect on the critical surface of the mechanical strains, we use the methodology defined in [4], adding a few steps to take into account irreversible effects on the strands before powering. The procedure is the following: 1) Measure the strand critical current as function of field, temperature and strain; 2) Fit the exponential scaling law to the measurements; 3) Use the critical current measurements to define a strain function limit for the irreversible strains; 4) Compute magnetic field and strain in the superconducting elements; 5) Check the magnet against irreversible strain limits; 6) Compute the critical current for each strand.

The strain effects on the critical surface are introduced by the strain function $s(\varepsilon)$, which is computed here using the exponential scaling law [1]:

$$s(\boldsymbol{\varepsilon}) \equiv \frac{B_{c2}(0,\boldsymbol{\varepsilon})}{B_{c2}(0,0)} = \frac{e^{-C_1 \frac{J_2+3}{J_2+1} J_2} + e^{-C_1 \frac{I_1^2+3}{I_1^2+1} I_1^2}}{2} \quad (1)$$

where $\boldsymbol{\varepsilon}$ is the strain tensor, $B_{c2}(T,\boldsymbol{\varepsilon})$ is the upper critical field as a function of strain and temperature, C_1 is a constant derived from critical current measurements performed on uniaxially loaded strands; I_1 is the first invariant of the strain tensor and J_2 is the second invariant of its deviatoric part.

The pinning force can be computed as follows:

$$F_p = J_c(B,T,\boldsymbol{\varepsilon}) \times B = C g(s(\boldsymbol{\varepsilon})) h(t) b^p (1-b)^q \quad (2)$$

where b is the reduced field and t the reduced temperature, defined as a function of the critical temperature $T_c(\varepsilon)$ and critical field B_{c2}.

$$T_c(\boldsymbol{\varepsilon}) = T_c(0) s(\boldsymbol{\varepsilon})^{\frac{1}{w}} \qquad t = T/T_c(\boldsymbol{\varepsilon}) \quad (3)$$

$$B_{c2}(T,\boldsymbol{\varepsilon}) = B_{c2}(0,0) s(\boldsymbol{\varepsilon})(1-t^{\nu}) \qquad b = B/B_{c2}(T,\boldsymbol{\varepsilon}) \quad (4)$$

Because of the differential thermal contraction between the different materials composing the strand, the Nb_3Sn filaments are not in a free state before powering. The effect is introduced with an offset on the longitudinal and transversal strain. Data shows that this effect can be summarized in a single parameter, for example the residual longitudinal strain ε_{l0}, and that the effect on the transversal strain is simply:

$$\varepsilon_{t0} = -\nu \varepsilon_{l0} + K \quad (5)$$

where ν is the Nb_3Sn Poisson's ratio and K a fitting parameter equal to 0.1 [1].

The critical current in each strand is finally computed as the average on each superconducting region [4].

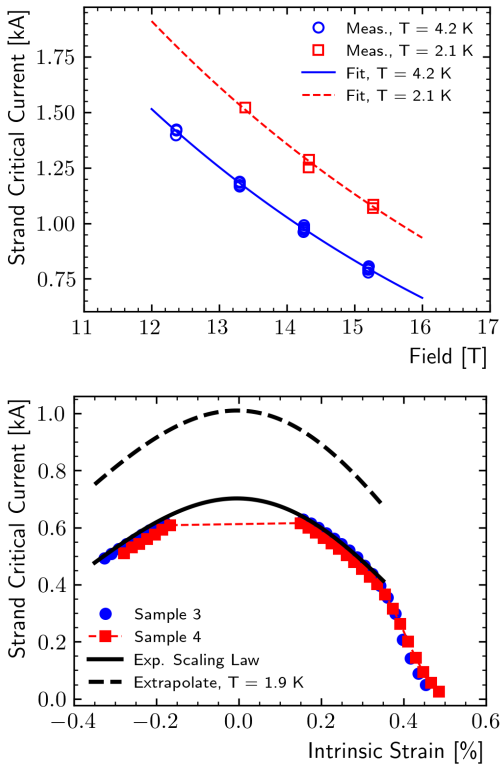

Fig. 2. Critical current measurements on strands as a function of the temperature and the background magnetic field (top, multiple samples with the same heat treatment), and as a function of the intrinsic strain, at 16 T and 4.2 K (bottom, two different samples), along with the fitting results. The dashed line on the bottom plot represents the extrapolated critical current at 1.9 K.

TABLE II
Fitting Results

Non-strain Parameters			Strain Parameters		
Parameter	Unit	Value	Parameter	Unit	Value
C	kA	111.4	C_1	/	0.86
B_{c20}	T	30.06	ε_{l0}	%	-0.2
T_{c0}	K	17.40	$s(\varepsilon)_{irr}$	/	0.85

IV. Critical Surface Parametrization

The computation of the pinning force from Eq. 2 requires 5 fitting parameters. These can be divided in two groups: non-strain related $[C, B_{c2}(0,0), T_c(0)]$ and strain related $[C_1, \varepsilon_{l0}]$. Further to this, the methodology requires the definition of a strain function limit for the irreversible degradation onset, $s(\varepsilon_{irr})$. To obtain these parameters, two sets of measurements were performed, with results shown in Fig. 2: as a function of the field, with constant strain and variable temperature, and as a function of the intrinsic strain, under a field of 16 T and a temperature of 4.27 K. For the latter measurements, a Cu-Be Walters spring was used to strain the samples. More information on the measurement apparatus can be found in [12].

Following the logical division between the parameters, and the distinction between the experiments, the fitting was performed in two steps: first, the non-strain related parameters were calibrated using the $I_c(T,B)$ measurements, and then the

strain related parameters were calibrated on the $I_c(\varepsilon)$ data. This procedure is slightly different from the one proposed in [13], where all the data is fitted at the same time. This procedure could not be adopted as two different set-ups are used for the two measurements, which also means that the initial strain ε_{l0} will be different for the two data sets. As the exponential scaling law is only valid in the reversible region, the Walters spring measurements were cut at the knee/cliff where irreversible effects appeared [12]. The measurements were corrected in order to keep track of strand self-field B_s with the following equation:

$$B_s = \mu_0 I(0.4/\phi_s - 0.1)/1.8 \tag{6}$$

where ϕ_s is the strand diameter, and μ_0 the vacuum permeability.

The fitting results are shown in Fig. 2, and the fitting parameters are reported in Table II. Of particular interest is the value of C_1, as this parameter represents the strain sensitivity of the strand: a comparison with the available literature data [1] shows that this value is higher than average. The fitting value ε_{l0} was found to be very close to 0 for the strain measurement setup. This value, however, cannot be used directly for the magnet analysis, as the differential thermal contraction between the spring and the strand introduces an offset that will be different to the one that the strands will experience in the actual magnet. As a consequence, a parametric investigation of its effect on magnet performances was performed (see Section V-D).

The Walters spring measurements identified an irreversibility cliff at a strain of 0.3%. This corresponds, with the C_1 parameter from the fitting, to a strain function of 0.85. At the moment, there is no experimental proof that filaments will fail when this threshold is reached, independently of the loading condition. However, a similar value of the strain function was found for the higher stress levels in the sample holder MQXF cable test, where a small amount of irreversible degradation was found [3], [14].

V. Critical Current Computation

A 2D FE magneto-mechanical model of the dipole was used to extract the current and strain on each strand. The model was built following a strategy consistent with the one proposed in [3], [4]. The model geometry can be seen in Fig. 1. The material properties for the coil components can be found in [3]. The mechanical model followed the life cycle of the magnet, simulating the room temperature loading, cool-down and powering up to 16 T.

A. Load Line Margin

The strain function was computed on all the strands at 16 T (see Fig. 3, bottom). Two strands of interest were selected for further analysis: one with high field / low stress, on the outer coil pole turn (max field), and one from a dangerous (high stress) area in the low field region. The strain function variation as a function of the magnet current for these strands is shown in Fig. 4: on the high field region $s(\varepsilon)$ increases gradually with the magnet current, and does not see a significant variation after 10 kA. In the low field region sees instead a continuous reduction as the e.m. forces increase. Therefore, the margin on the pole turns is not affected by strain, while the margin in the low field region is reduced with respect to the strain-free case. The short sample limit for each strand, as a function of field and strain was computed. A conservative 5% cabling degradation was added to the fitting

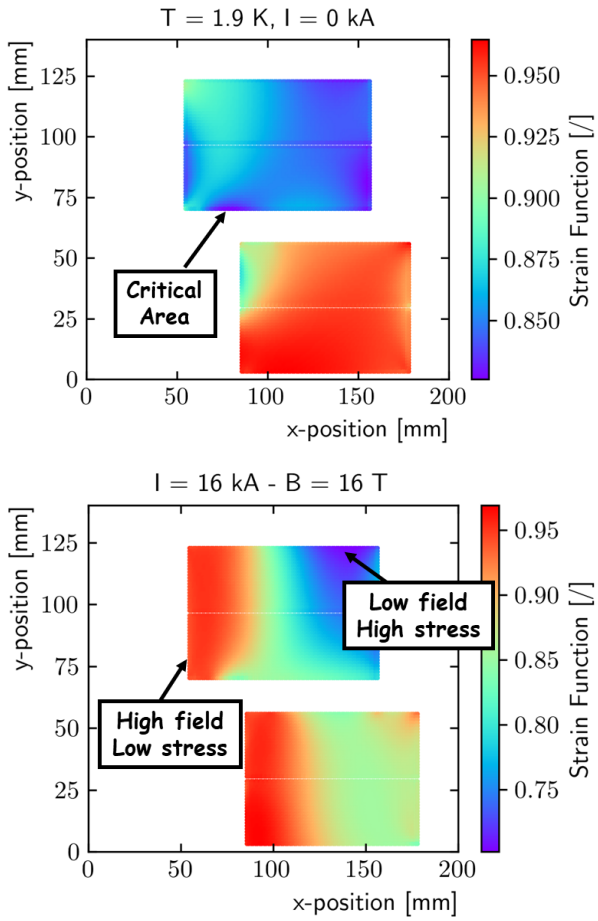

Fig. 3. Strain function after magnet cooldown (top), used to check against irreversible degradation, and at 16 T (bottom), necessary to compute the critical current margin at the target field.

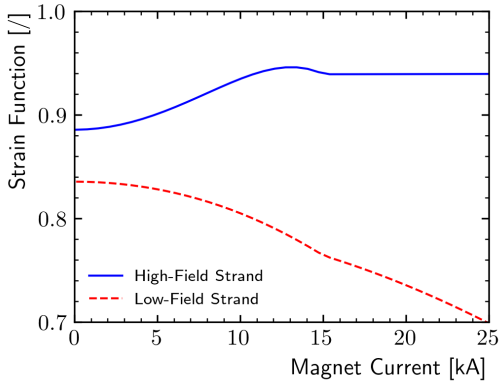

Fig. 4. Strain function as a function of the magnet current on the high-field and low-field strands identified in Fig. 3.

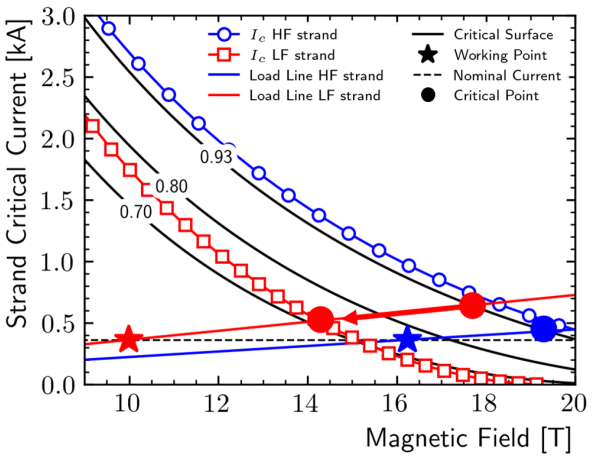

Fig. 5. Load lines of the high field / low stress and low field / high stress regions, at 1.9 K. The critical surface is plotted for three values of the strain function, 0.7, 0.8 and 0.93. The latter includes only the strain induced in a free strand by the differential thermal contraction. The full markers represent the critical current on the strands with/without mechanical strain effects.

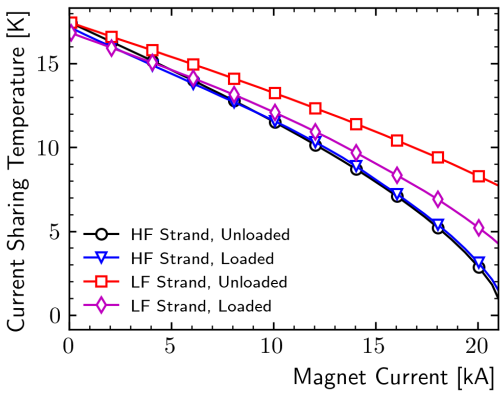

Fig. 6. Current sharing temperature on the high field / low stress and low field / high stress regions, as a function of the magnet current.

parameters of Table II. Fig. 5 shows the load line evolution on the two identified regions: the magnet operates at 80% of the short sample limit in the high field/low stress region, and at 68% in the low field/high stress region. Including only the strain due to the differential thermal contraction effects inside the strand, the operating point would have been 83% and 56%. This means that the high field strand sees a 3% margin increase, while the low field strand is affected by a 12% reduction.

B. Temperature Margin

The critical strand temperature, computed as a function of the magnet current, is shown in Fig. 6 for the low field and high field strands, with (loaded) and without (unloaded) strain effects. The variation of the margin is negligible in the high field strand. However, in the low field, high stress strand, the temperature margin at 16 T is equal to 8.3 K, while it would have been 10.4 K with no strain effects.

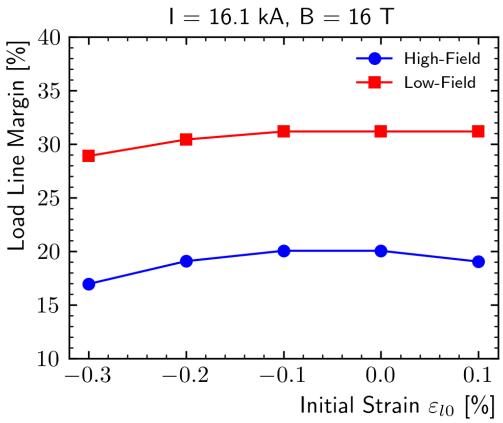

Fig. 7. Variation of the load line margin in the high field and low field regions as a function of the initial strain parameter ε_{l0}.

C. Irreversible Degradation After Cooldown

Potential irreversible degradation effects during assembly and cool-down were checked using the strain function threshold defined in Section IV. The strain function averaged on each strand after cool-down is shown in Fig. 3 (top): the critical area is the lower side of the upper coil, where $s(\boldsymbol{\varepsilon})_{CD}$ is equal to 0.83 and slightly below the threshold of 0.85 mentioned in Section IV.

D. Effect of the Initial Strain

As underlined previously, the actual value of ε_{l0} cannot be obtained from the Walter-Spring measurements and will depend on the strand environment in the magnet (e.g. insulation thickness). Based on the available literature data, this parameter can range between -0.1% and -0.3%. The effect on the load line margin is shown in Fig. 7, where also an extreme case with $\varepsilon_{l0} = 0.1\%$ was considered. The initial strain effect is small: the margin ranges from 17% to 20% on the high field region and from 29% to 31% in the low field one.

VI. Conclusion

We have used the exponential strain function to consider the effect of the strain on the expected performances of a 16 T test facility dipole. Critical current measurements were performed and the data was fitted to find the parameters defining the critical surface as a function of current, field, temperature and strain.

A 2D finite element model was then used to compute the field and strain inside each of the dipole strands. The results suggest that the magnet can reach 16 T with significant margin: the working point in terms of load line margin is 20% in the high field/low stress region, and 32% in the low field/high stress region. For the first time, a 3D irreversibility limit was defined using the strain function. The degradation threshold was found at a strain function of 0.85. The model shows that, after cooldown and with full prestress for 16 T operation, some strands are close to irreversible degradation in the low field region.

REFERENCES

[1] B. Bordini, P. Alknes, L. Bottura, L. Rossi, and D. Valentinis, "An exponential scaling law for the strain dependence of the Nb_3Sn critical current density," en, *Superconductor Science and Technology*, vol. 26, no. 7, p. 075 014, 2013.

[2] T. Wang, L. Chiesa, M. Takayasu, B. Bordini, and A. Principle, "Modeling of the critical-current behavior of Nb_3Sn subsized cables under transverse load using 2D finite element analysis and a strain scaling law," *Ieee Transactions on Applied Superconductivity*, vol. 24, no. 3, pp. 1–5, 2014.

[3] G. Vallone, B. Bordini, and P. Ferracin, "Computation of the reversible critical current degradation in Nb_3Sn rutherford cables for particle accelerator magnets," English, *Ieee Transactions on Applied Superconductivity*, vol. 28, no. 4, p. 4 801 506, 2018.

[4] G. Vallone *et al.*, "A methodology to compute the critical current limit in Nb_3Sn magnets," en, *Superconductor Science and Technology*, 2020.

[5] P. Ferracin *et al.*, "Mechanical design of HD2, a 15 T Nb_3Sn dipole magnet with a 35 mm bore," *IEEE Transactions on Applied Superconductivity*, vol. 16, no. 2, pp. 378–381, 2006.

[6] E. Rochepault *et al.*, "Mechanical analysis of the FRESCA2 dipole during preload, cool-down, and powering," *IEEE Transactions on Applied Superconductivity*, vol. 28, no. 3, pp. 1–5, 2018.

[7] H. Felice *et al.*, "Performance of a Nb_3Sn quadrupole under high stress," vol. 21, no. 3, pp. 1849–1853, 2011.

[8] G. V. Velev *et al.*, "Design and construction of a high field cable test facility at fermilab," *IEEE Transactions on Applied Superconductivity*, vol. 31, no. 5, pp. 1–4, 2021.

[9] S. Caspi *et al.*, "The use of pressurized bladders for stress control of superconducting magnets," *IEEE Transactions on Applied Superconductivity*, vol. 11, no. 1 II, pp. 2272–2275, 2001.

[10] G. Vallone *et al.*, "Magnetic and mechanical analysis of a large aperture 15 T cable test facility dipole magnet," *IEEE Transactions on Applied Superconductivity*, vol. 31, no. 5, pp. 1–6, 2021.

[11] J. L. R. Fernández *et al.*, "Engineering design of a large aperture 15 T cable test facility dipole magnet," *IEEE Transactions on Applied Superconductivity*, vol. 32, no. 6, pp. 1–5, 2022.

[12] N. Cheggour, T. C. Stauffer, W. Starch, L. F. Goodrich, and J. D. Splett, "Implications of the strain irreversibility cliff on the fabrication of particle-accelerator magnets made of restacked-rod-process Nb_3Sn wires," en, *Scientific Reports*, vol. 9, no. 1, p. 5466, 2019.

[13] J. Ekin *et al.*, "Extrapolative scaling expression: A fitting equation for extrapolating full Ic (B,T,ε) data matrixes from limited data," *IEEE Transactions on Applied Superconductivity*, vol. 27, no. 4, pp. 1–7, 2017.

[14] B. Bordini, P. Alknes, A. Ballarino, L. Bottura, and L. Oberli, "Critical current measurements of high-Jc Nb_3Sn rutherford cables under transverse compression," *IEEE Transactions on Applied Superconductivity*, vol. 24, no. 3, pp. 1–5, 2014.